Thermocline Thermal Storage Using a Packed bed of Moroccan Rocks

K El Alami[1], M Asbik[1], N Zari[2] and S Rachidi[3]

[1] ERTE, Ecole Normale Supérieure de l'Enseignement Technique, Université Mohammed V, Rabat, Morocco.
[2] Moroccan Foundation for Advanced Science Innovation and Research (MAScIR)
[3] Institut de Recherche en Energie Solaire et Energies Nouvelles (IRESEN), 16, Rue Amir Sidi Mohamed, Souissi, Rabat, Morocco.

E-mail: [1]dijaelalami@gmail.com , [1] mohamed. asbik@um5.ac.ma, [2]n.zari@mascir.com,

[3]rachidi@iresen.org

Abstract. This work is a contribution to the numerical study of the thermal behavior of a thermocline storage system. The energy conservation equations associated with their boundary conditions, have been solved numerically in the two filed media solid (rock) and fluid (HTF) constituting the packed bed thermal energy storage (TES). A parameter study of the packed bed dimensions, fluid flow rate, particle diameter and the ratio $\frac{H}{D}$ were carried out to evaluate the charging/discharging profiles of storage system. The results have been validated and they are in good agreement with the literature.

Keywords- Thermocline; Packed Bed; Rock; Heat Transfer Fluid.

1. Introduction

Today, concentrating solar power (CSP) technology is one of the most promising technologies for electricity production. However, the intermittency of this clean energy remains a technological challenge to be met by developing high temperature thermal storage systems (TES) [1-2]. These systems offer the possibility of retrieving the stored energy during periods of high demand and/or in the absence of the source of solar energy (nights and/or periods under adverse climatic conditions) [3].

Currently, the most mature TES system technology (Andasol, Noor 1,...) is based on the use of two tanks (hot/cold) in which a fluid (molten salt) circulates allowing the heat storage (charging/discharging) by using the principle of sensible heat [4]. This technology is quite expensive since it represents an initial investment ranging between 15 and 20% of the solar power plant cost [5-6]. Recently, a single thermal storage tank system has been developed at the laboratory scale "Sandia". Compared to this configuration, the TES single tank system can save up to 35% of the investment cost [7-8].Thus, Pacheco et al. [8] developed a packed bed TES system at pilot scale filled with rocks and showed that quartzite and silica sand are the most suitable storage materials in combination with molten salt (Hitec XL) as working fluid. In the same context, Zanganeh et al. [9] studied a packed bed of rocks at a temperature up to 650°C, using air as the heat transfer fluid (HTF), and described a storage system that could be used in a CSP. In 2016, Grirate et al. [10] compared the potential of six rock types proposed as storage

materials and their compatibility with synthetic oil as HTF. The thermal properties of these rocks were evaluated experimentally in a temperature range between 25°C and 300 °C.

In this paper, a numerical simulation of the thermal behavior of a thermocline storage system was performed. A local rock "granite" is used as a storage material and "Therminol VP1" as a heat transfer fluid, the effects of different parameters namely: equivalent diameter of the rocks d, the aspect ratio $\frac{H}{D}$, mass flow rate per unit cross section G, were studied to determinate those which gives better performances of the storage system TES.

2. Problem Formulation

2.1. Physical model

The studied storage device (packed bed) is illustrated in the Fig. 1a. It is a cylindrical tank filled with Moroccan rock (Granite) containing void spaces that are occupied by a heat transfer fluid (Therminol VP1). Thermal storage is carried out via the principle of thermocline which is based on a thermal gradient to separate the hot zone from the cold zone inside the considered system. Thermal heat storage consists of one cycle (or more) which is a physical process composed of two stages, namely, the charging and the discharging periods [11]. Fig. 1b shows the operating principle of the thermocline zone, which can represents up to one third of the height of the tank. This zone moves downward during the charging stage whereas it progresses upward when discharging phase takes place. In order to store the heat energy (charging phase), the hot fluid at a temperature T_h is introduced into the upper part of the tank and it flows downward through the packed bed and hence the cold fluid escapes through the diffuser of the lower part. During this step, the hot fluid transfers the heat energy to the storage materials, initially at the temperature T_c, up to a temperature T_h. In contrast to this, the direction of HTF is reversed during the heat retrieve stage since the cold fluid penetrates via the lower part of the tank and then receives the stored energy from rocks. The recovered energy will be forwarded to the power block of a concentrating solar power plant (CSP).

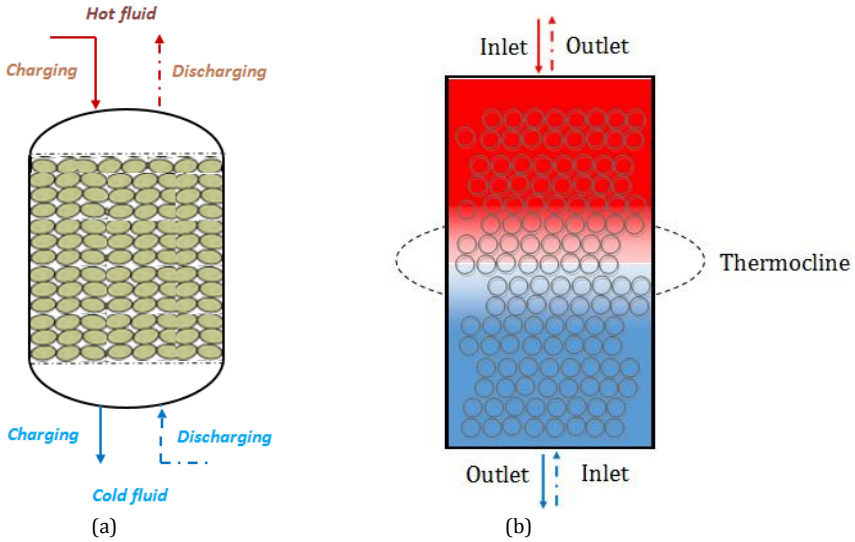

Figure 1. Operating principle of a thermocline storage Tank.

2.2. Hypotheses

In this study, the following hypotheses were made:

- the system is assumed to be one-dimensional;
- for the solid particles, lumped system model is considered (the Biot number, $B_i = \frac{h_p d_p}{k_s}$, should be less than 1);

- the packed bed has an infinite effective thermal conductivity in the radial direction;
- there is no temperature gradient inside the particles;
- the top and bottom of the system are insulated;
- radiation heat transfer is negligible;
- the heat generation inside the packed bed is not taken into consideration.

2.3. Mathematical modelling

The thermal behavior of the tank was developed and simulated by the Schumann equations [12], which describe the heat transfer between the fluid and a compact bed. Thus, the dimensionless conservation equations are written in the fluid and solid phases respectively:

$$\frac{\partial \theta_f}{\partial \tau} + \frac{\partial \theta_f}{\partial X} = \frac{1}{P_{ef}} \frac{\partial^2 \theta_f}{\partial X^2} + S_{tf,s}(\theta_s - \theta_f) + S_{tp}(\theta_\infty - \theta_f) \quad (1)$$

$$\frac{\partial \theta_s}{\partial \tau} = \frac{1}{P_{es}} \frac{\partial^2 \theta_s}{\partial X^2} + kS_{tf,s}(\theta_f - \theta_s) \quad (2)$$

Where:

$$\theta = \frac{T - T_{amb}}{T_h - T_{amb}}; \qquad X = \frac{x}{H}; \qquad \tau = \frac{t\, v_f}{H}$$

Before discretizing the conservation equations (1-2), the storage tank is divided into N vertical regular layers. On the other hand, the initial and boundary conditions associated with the above equations are:

1) The initial temperature distributions of the solid and fluid phases should be specified for the N layers.
2) The inlet temperature of the fluid phase should be specified for each time step $\Delta\tau$.
3) Adiabatic conditions for the fluid phase at the outlet of the physical domain "layer N+1", for the charging phase are expressed by Eq. (3):

$$\frac{\partial \theta_f(X=1)}{\partial X} = 0 \quad (3)$$

4) Adiabatic conditions for the solid phase at the inlet and outlet of the physical domain "Layers 0 and N+1" respectively for the charging phase, are represented by Eq. (4):

$$\frac{\partial \theta_s(X=0)}{\partial X} = \frac{\partial \theta_s(X=1)}{\partial X} = 0 \quad (4)$$

The previous equations have been solved numerically by using the implicit finite difference method [13].

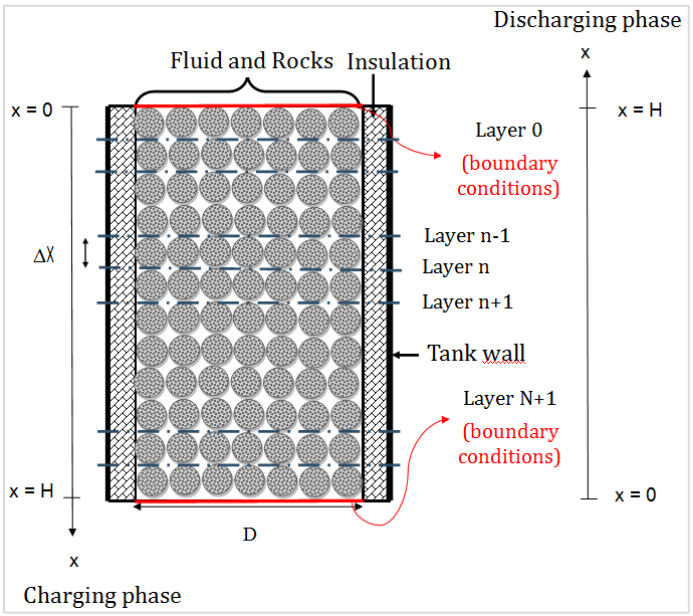

Figure 2. Packed bed storage system scheme.

3. Results and discussion

3.1. Validation of the simulation tool

The numerical simulation was carried out using the MATLAB (R2011b) software, based on the mathematical model presented above. The numerical results have been validated using the experimental data of Pacheco et al [8] which consists in discharging phase during two hours. Dimensions, operating parameters and the thermo-physical properties of the two field media fluid and solid were evaluated according to the reference of Van Lew et al. [14].

Figure 3. exhibits the evolution of numerical temperature profiles against the experimental results of Pacheco et al. [8]. It is clear that numerical and experimental results are in good agreement. Consequently, the model could be able to predict the thermal behavior of a single tank storage unit.

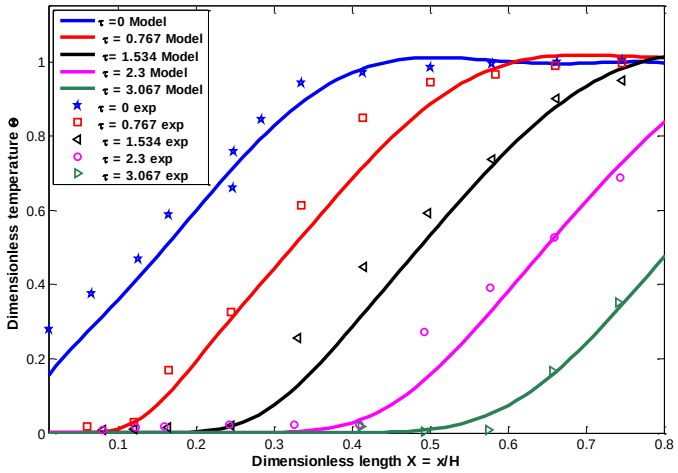

Figure 3. Comparison between numerical results and experimental measurements of Pacheco et al. [8]. Exp: experimental measurements, Model: numerical results.

3.2. Parametric study

In this work, the parametric study was carried out for two different circumstances:

- The first thermal cycle (3h charging/ 3h discharging);

- A series of five consecutives thermal cycles (3h charging/ 3h discharging).

The thermo-physical properties of HTF are presented in Table 1 whereas the thermo-physical properties of rock, the dimensions of the storage system and the operating parameters used in the simulation study are listed in Table 2.

Table 1: Thermal properties of heat transfer fluid [11]

Heat transfer fluid	Oil : Therminol VP1
Composition	73.5% diphenyl oxide and 26.5% biphenyl oxide
Temperature of solidification	12 °C
Maximum temperature of operation	400 °C
Vapor pressure	10.9 bars at 400 °C
Thermal capacity (250 °C)	1.89 MJ/m^3.K
Thermal conductivity (250 °C)	0.106 W/m.K
Dynamic viscosity (250 °C)	0.29 mPa.s
Availability	Low
GHG	3 kg CO_2eq kg^{-1}
Degree of Dangerousness	High

Table 2: Dimensions and operating parameters of the cylindrical TES system [15-17]

Dimensions	Value	Unit
Tank height	3	m
Tank diameter	2	m
Surface area	3.1416	m^2
Rock diameter	0.03	m
ε	0.27	--
Operational parameters		
$\dot{m}_{ch/disch}$	0.3	kg/s
$t_{ch/disch}$	3	h
T_{amb}	298	K
T_h	523	K
U	0.678	W/m^{2}K
ρ_s	2600	kg/m^3
C_p	820	J/ kg K
K_s	2.8	W/m K
n	100	--

Figures 4a and 4b exhibit dimensionless temperature distributions which correspond to solid and fluid field media, during a single cycle (a: charging, b: discharging). According to these figures, it is obviously evident that after each period of charging or discharging t = 0.5, 1, 2 and 3 hours, the HTF and the storage material have practically the same temperature ($T_f \approx T_s$). Moreover, in case of charging phase, inlet of the tank, these temperatures have the same value T_h ($\theta \approx 1$). Contrary to this, they take the value of ambient temperature T_{amb} ($\theta \approx 0$) at the inlet of the discharging phase. Furthermore, it is also clear that in the thermocline region, the falling temperature is very significant. The thickness of this zone depends simultaneously on the heat transfer fluid, the storage materials and time of charging/discharging of storage system TES.

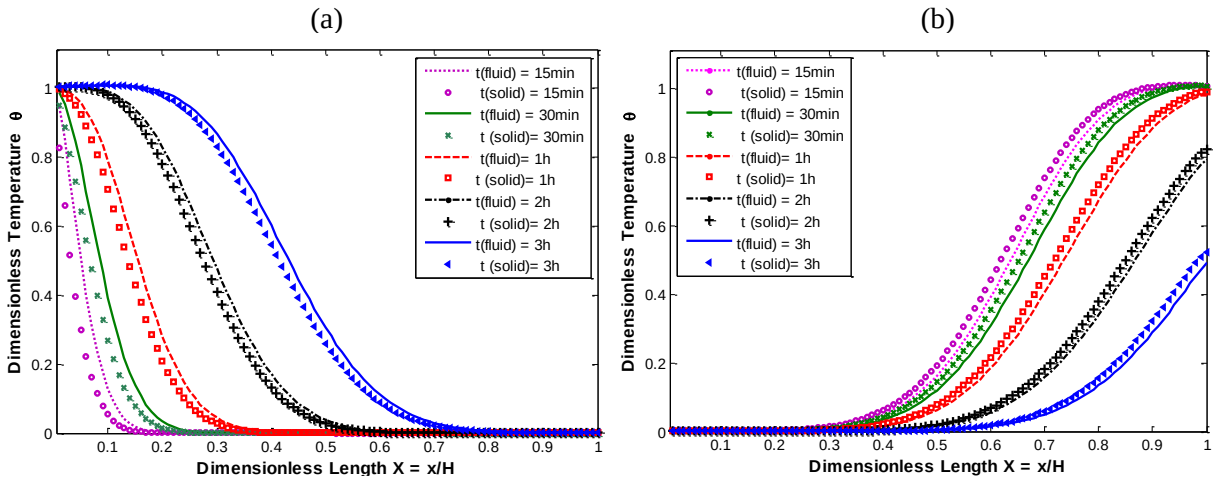

Figure 4. Dimensionless temperature profiles of the fluid and solid phases along the storage tank of the single cycle: (a) charging / (b) discharging periods.

3.3. Effects of the parameters ($\frac{H}{D}$, d, G) on the dimensionless temperature of HTF and rock

As expected, in the case of the charging process, the dimensionless temperatures evolutions of solid follow the classical behavior of thermal conduction regardless of whatever the position (Figures 5a-b: X=0.2 or X=0.8). It is clear from the curves of these figures that, at a given time, solid temperature values increase with the aspect ratio $\frac{H}{D}$, and this increase are more pronounced for its high values. Also, the variation of this parameter has a tangible effect on the thermal diffusion regime (transient regime or steady state). Thus, the time required to reach the steady state is even shorter if this ratio is high. These results can be explained by the fact that the cross section of the HTF becomes narrow since the tank height is kept constant and its diameter is varied. As for the Figures 6a-b, they show dimensionless temperature distributions of the fluid after the first (Figure 6a) and fifth (Figure 6b) thermal cycles with respect to dimensionless coordinate X. It should be noted that the augmentation of the aspect ratio accelerate the saturation of the system and hence the thermal equilibrium between rocks and the HTF (case of $\frac{H}{D} = 3$). On the other hand, it is easy to see that in the case where $\frac{H}{D} < 3$ the heat is gradually stored which generates the temperature homogenization inside rocks: $B_i < 1$ (see Figure 8a).

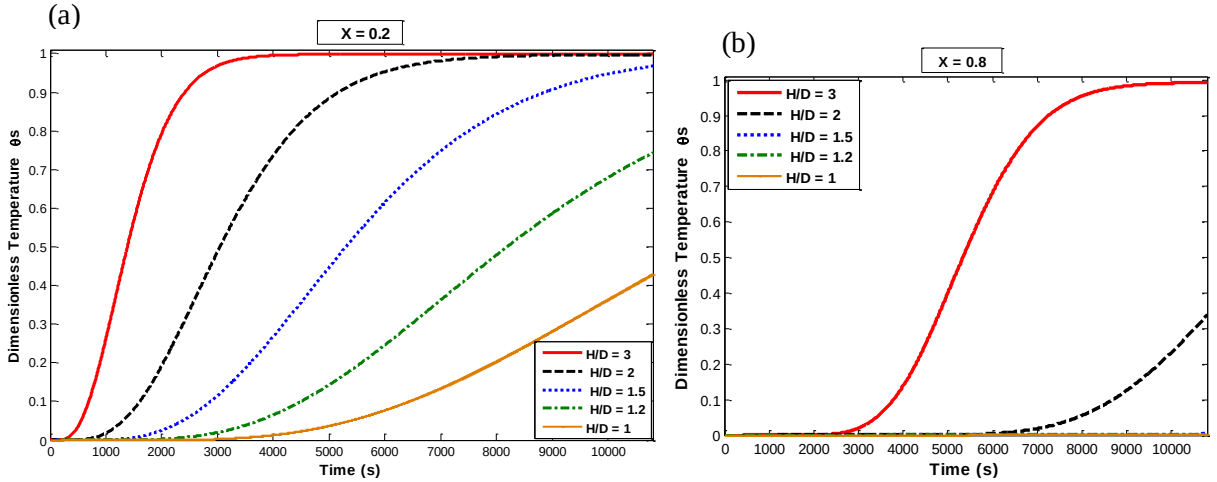

Figure 5. Dimensionless temperature profiles of the solid at the dimensionless positions $X = 0.2$ and $X = 0.8$ during the charging period: The effect of aspect ratio variations.

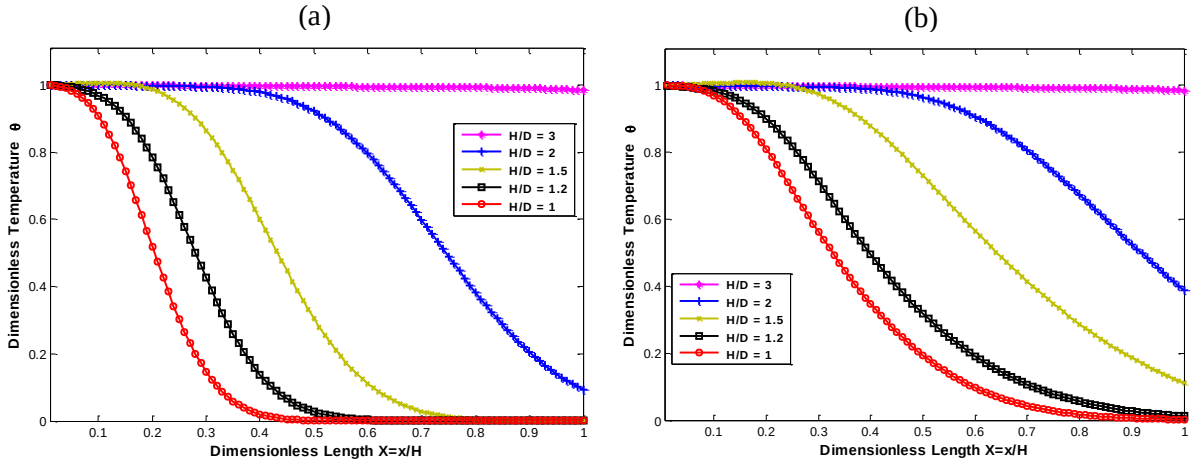

Figure 6. Dimensionless temperature distributions of the fluid along the storage tank at the end of the charging period: (a) first cycle, (b) fifth cycle.

Figures 7a and 7b show the dimensionless temperature profiles of rock and HTF (Therminol VP1) at the end of the first and fifth charging processes, for different particle diameters d = 1mm to d = 7mm. The number of Biot was compared for all diameters and it was less than 1 (Figure 8b) and therefore the assumptions mentioned above are respected. Furthermore, the difference between the storage material (Granite) and heat transfer fluid temperature (Therminol VP1) noticeably narrows for smaller particle size, the thermocline zone is sharper through the length of the tank (Figure 7a).The same behavior is observed at the end of the 5th cycle. Indeed, the small size of the particles allows a more efficient heat transfer between the solid and fluid due to the high specific exchange surface and the high coefficient of convective heat transfer.

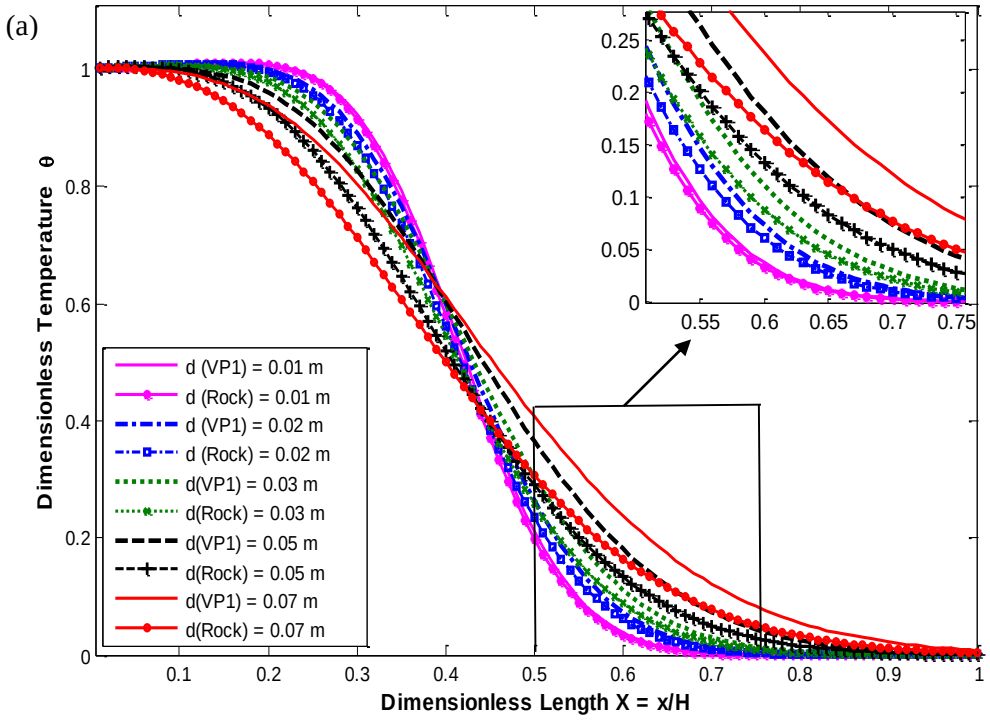

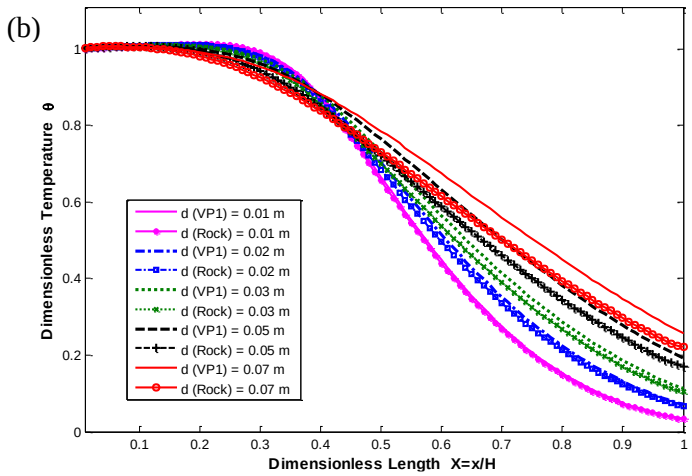

Figure 7. Effect of rock diameter variation on the dimensionless temperature profiles of the fluid and solid phases along the storage tank at the end of the charging period: (a) first cycle, (b) 5th cycle

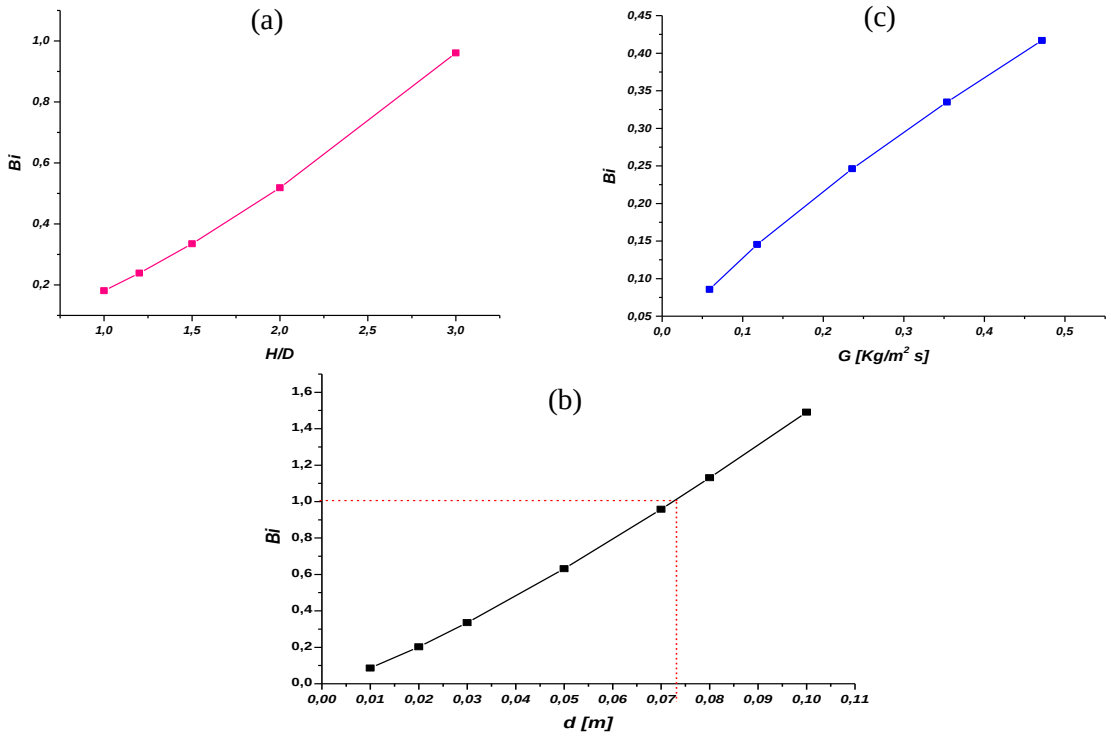

Figure 8. Variations of Biot number at the end of the charging period with respect to : (a) aspect ratio $\frac{H}{D}$, (b) particle diameter d, and (c) mass flow rate per unit cross section G.

Figures 9a and 9b exhibit the dimensionless temperature distributions inside the rock (granite) and in the oil (TerminolVP1) along the storage tank at the end of the first charging process (3h) and the 5th thermal cycle, respectively, for different values of G (0.058 kg/m^2 s ≤ G ≤0.047 kg/m^2 s). For both cases, higher flow rate leads obviously to higher temperatures at the packed bed. At the end of the first cycle, for the maximum mass flow per unit cross section, the temperature at the position $X = 0.5$ reaches 190°C ($\theta \approx 0.62$), while it remains at ambient temperature ($\theta \approx 0$), for G = 0.05 kg/m^2 s and G = 0.23 kg/m^2 s (Figure 9a). In addition, the increase of the thermocline thickness can be seen as the oil mass flow increases. Furthermore, the temperature gradient zone is larger for the 5th cycle than the first one.

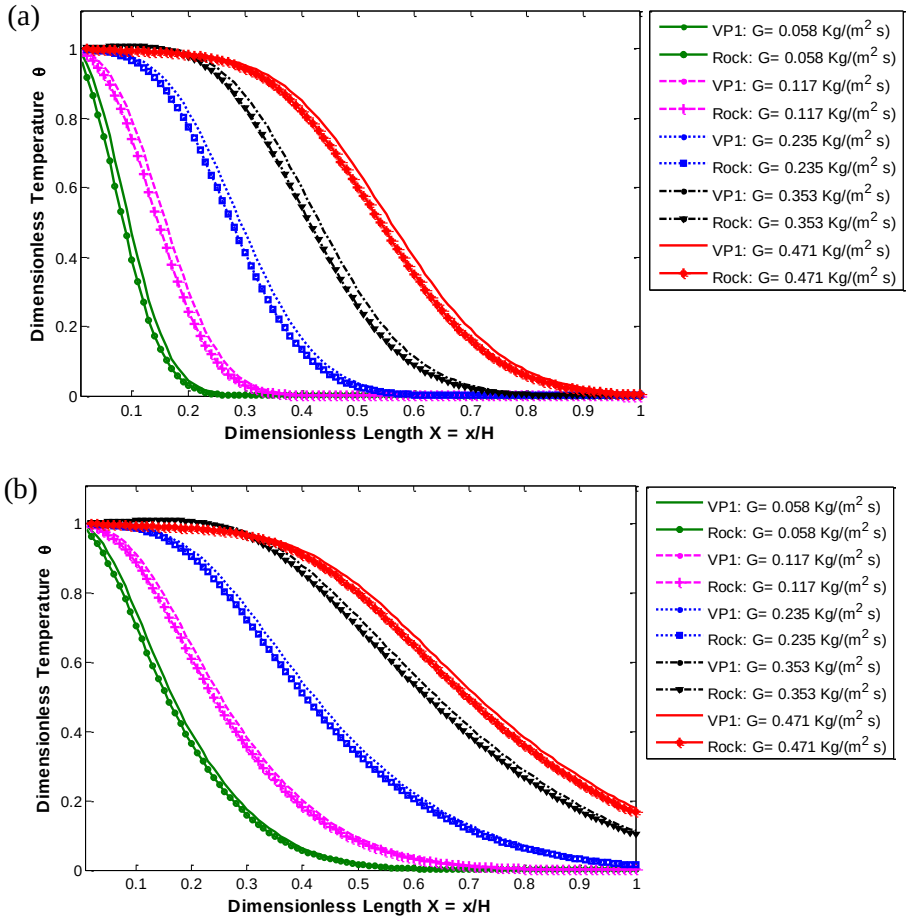

Figure 9. Effect of mass flow rate per unit cross section G on the dimensionless temperature profiles of the fluid and solid phases along the storage tank at the end of the charging period: (a) first cycle, (b) 5th cycle.

4. Conclusion

In this work, a mathematical model of heat transfer in a packed bed TES thermocline system has been developed. A simulation tool was conducted in the MATLAB software environment and validated experimentally. A parametric study of the packed bed in terms of aspect ratio, particle diameter and fluid mass flow rate was carried out during charging/discharging periods and also thermal cycling operation of a thermocline storage system.The most relevant property of the storage material is the volumetric heat capacity, while the thermal conductivity of the solid has only a minor effect. In the range of particle sizes considered, the dimensionless temperature profiles of rock and oil is found considerably better for the smallest particle size of the 5thcycle. High fluid mass flow rate and high values of aspect ratio lead to increase in temperature.

References

[1] Wang ZF 2010, Prospectives for China's solar thermal power technology development. *Energy*, **35**: 4417–20.
[2] He YL, Xiao J, Cheng ZD, Tao YB, Mcrt A, VM F, et al. 2010, A MCRT and FVM coupled simulation method for energy conversion process in parabolic trough solar collector. *Ren. Energy*; **36**: 976–85.
[3] Relloso S, Garcia E 2015, Tower technology cost reduction approach after gema solar experience. *Energy Proc*. **69**, 1660–1666.

[4] Gil A, Medrano M, Martorell I, Lázaro A, Dolado P, Zalba B and Cabeza LF 2010, State of the art on high temperature thermal energy storage for power generation:1. Renew. *Sust. Energy Rev.* **14** 31–55.
[5] Herrmann U, Kelly B, and Price 2004, Two-tank molten salt storage for parabolic trough solar power plants. *Energy*, **29**, 883–893.
[6] Angelini G, Lucchini A, and Manzolini G 2013, Comparison of thermocline molten salt storage performances to commercial two-tank configuration, *Energy Procedia*, **49**: 694–704.
[7] Kearney D, Kelly B, Herrmann U, Cable R and J. Pacheco 2004, Engineering aspects of a molten salt heat transfer fluid in a trough solar field. *Energy* **29**, 861–870.
[8] Pacheco JE, Showalter SK, Kolb WJ 2002, Development of a molten-salt thermocline thermal storage system for parabolic trough plants. *J Solar Energy Eng*; **124**:153–9.
[9] Zanganeh G, Pedretti A, Zavattoni S, Barbato M, et al. 2012, Packed-bed thermal storage for concentrated solar power-pilot scale demonstration andindustrial-scale design. *Sol. Energy* 86 (10) 3084–3098.
[10] Grirate H, Agalit H, Zari H, Elmchaouri A, Molina S and Couturier R 2016, Experimental and numerical investigation of potential filler materials for thermal oil thermocline storage, *Sol. Energy* **131**: 260-274.
[11] Hoffmann J.F 2015, Stockage thermique pour centrale solaire thermody-namique à concentration mettant en œuvre des matériaux céramiques naturels ou recyclés, *Doctoral dissertation*, Perpignan.
[12] Schumann, T.E.W. 1929, Heat transfer: a liquid flowing through a porous prism. J. Frankl. Inst. 208, 405–416. .http://dx.doi.org/10.1016/S0016-0032(29)91186-8.
[13] Dale A. Anderson et al. 1984, Computational fluid mechanics and heat transfer, Series in computational methods in mechanics and thermal sciences.
[14] Van Lew, J.T., Chan, C.L., Karaki, W., Stephens, J 2011, Analysis of heat storage and delivery thermocline tank having solid filler material. *J. Sol. Energy Eng*. **133**, 021003-1–021003-10.
[15] Eppelbaum L, Kutasov I, Pilchin A 2014, Thermal Properties of Rocks and Density of Fluids. *Appl. Geotherm*., Springer, Berlin, Heidelberg, pp. 99–149.
[16] Miao S.Q, Li H.P, Chen G 2014, Temperature dependence of thermal diffusivity, specific heat capacity, and thermal conductivity for several types of rocks. *J.Therm. Anal. Calorim*. 115 1057–1063.
[17] Grirate H, Zari N, Elamrani I, Couturier R, Elmchaouri A, Belcadi S and P.Tochon 2014, Characterization of several Moroccan rocks used as filler material for thermal energy storage in CSP power plants. *Energy Procedia* **49** 810–819.

Nomenclature

Symbols

A	Surface area (m^2)
d	Rock diameter (m)
D	Diameter (m)
H	Height (m)
t	Time (s)
τ	Dimensionless time (–)
T	Temperature (K)
v	Velocity (m/s)
Q_m	Mass flow rate (kg/s)
G	Mass flow rate per unit cross section (Kg/m^2 s)
U	Overall heat transfer coefficient (w/m^2k)
x	Variable length (m)
X	Variable dimensionless length (–)
Bi	Biot number (--)
S_{t_w}	Stanton number of tank wall (–)
$S_{t_{f,s}}$	Stanton number fluid/solid (–)
P_{e_i}	Peclet number (i is f for fluid or s for solid)

Greek letters

θ	Dimensionless temperature (–)
k	Ratio of solid to fluid thermal conductivity (–)
ε	Porosity of the storage tank (–)

Subscripts

amb	Ambient
s	Solid
f	Fluid
w	Wall
h	Hot
c	Cold